THE JOURNAL OF PHYSICAL CHEMISTRY C
A JOURNAL OF THE AMERICAN CHEMICAL SOCIETY

pubs.acs.org/JPCC

Article

Ultrastrong Coupling Leads to Slowed Cooling of Hot Excitons in Few-Layer Transition-Metal Dichalcogenides

Published as part of The Journal of Physical Chemistry virtual special issue "Quantum Coherent Phenomena in Energy Harvesting and Storage".

Aaron H. Rose, Taylor J. Aubry, Hanyu Zhang, Derek Vigil-Fowler, and Jao van de Lagemaat*

Cite This: *J. Phys. Chem. C* 2022, 126, 8710–8719

Read Online

ACCESS | Metrics & More | Article Recommendations | Supporting Information

ABSTRACT: The excited-state dynamics of few-layer molybdenum disulfide (FL-MoS_2) are studied in conditions of strong light−matter coupling to plasmon polaritons. Hot carrier extraction in these systems has been proposed due to the observation of slow cooling of the high-energy C exciton relative to the bandgap A exciton. Here, we show that in conditions of ultrastrong coupling to plasmon polaritons, the lifetimes of the two slowest C exciton decay processes are extended by factors of 1.5 and 5.8 in FL-MoS_2. We hypothesize that strong coupling delocalization suppresses multiple decay mechanisms throughout the visible spectrum in MoS_2 such as defect scattering, intervalley scattering of band-nested excitations to the K-valley band edges, and exciton−exciton annihilation. We also find that decay from the upper to the lower hybrid mode is not ultrafast as seen in organic systems but in fact introduces an additional delay of ∼20 ps. Our observations show that strong coupling can be used to extend the lifetimes of hot excitons in FL-MoS_2 and potentially in other two-dimensional transition-metal dichalcogenides, with potential for above-bandgap photophysics and photochemistry applications such as hot carrier extraction, which could lead to more efficient solar energy conversion.

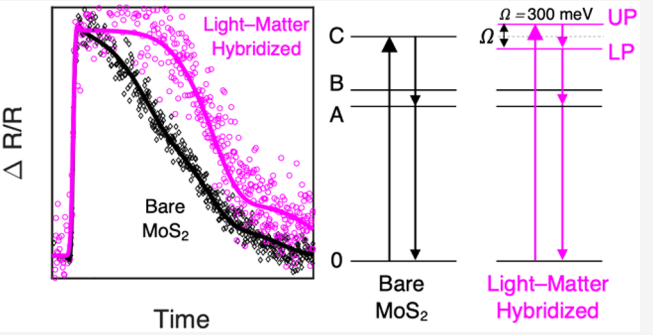

INTRODUCTION

Strong coupling of excitons and light into hybrid modes called exciton−polaritons is a quantum coherent phenomenon with a wide variety of applications from laser physics,[1−3] chemical reactivity control,[4−6] quantum information processing,[7] and energy conversion.[8] Under strong coupling conditions, resonant light (e.g., polaritons) and matter (e.g., excitons or molecular vibrations) modes of equal energy hybridize, resulting in split energy levels and coherent oscillation between the two new eigenstates. Strong coupling has led to exciting demonstrations such as polariton condensation and superfluidity,[9] modification of electronic properties such as the work function and mobility,[10,11] and control over chemical reaction rates and selectivity.[4,5]

Previously, the excitonic systems available for strong coupling studies were limited to quantum dots, organic semiconductors, or inorganic semiconductors at cryogenic temperatures.[12−14] Recently, strong coupling in inorganic semiconductors has been achieved at room temperature in the two-dimensional (2D) transition-metal dichalcogenides (TMDCs) with exciting results such as ultralow threshold polariton lasing with WS_2.[3] The 2D TMDCs are layered crystalline semiconductors attractive for their strong light−matter interactions arising from unique optoelectronic properties such as their excitonic fine structure and ultrathin, quantum confined nature. TMDCs exhibit sharp excitonic resonances, large optical absorption coefficients, and promising electronic properties. These materials can be made through a variety of nanofabrication processes, showing flexibility and promise toward device integration. Furthermore, strong spin−orbit interactions in TMDCs yield optically accessible states that are protected by spin−valley locking and may allow a route to all optical qubits.[15,16] Plasmonic strong coupling-modulated valleytronic emission has already been demonstrated toward this goal.[7]

However, short excited-state lifetimes limit the utilization of the TMDCs in these various applications. Thus, understanding and controlling carrier lifetimes is important. Toward this end, we focus on strong coupling as a control mechanism and target

Received: February 21, 2022
Revised: May 2, 2022
Published: May 17, 2022

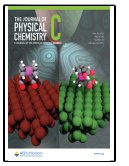

https://doi.org/10.1021/acs.jpcc.2c01262
J. Phys. Chem. C 2022, 126, 8710−8719

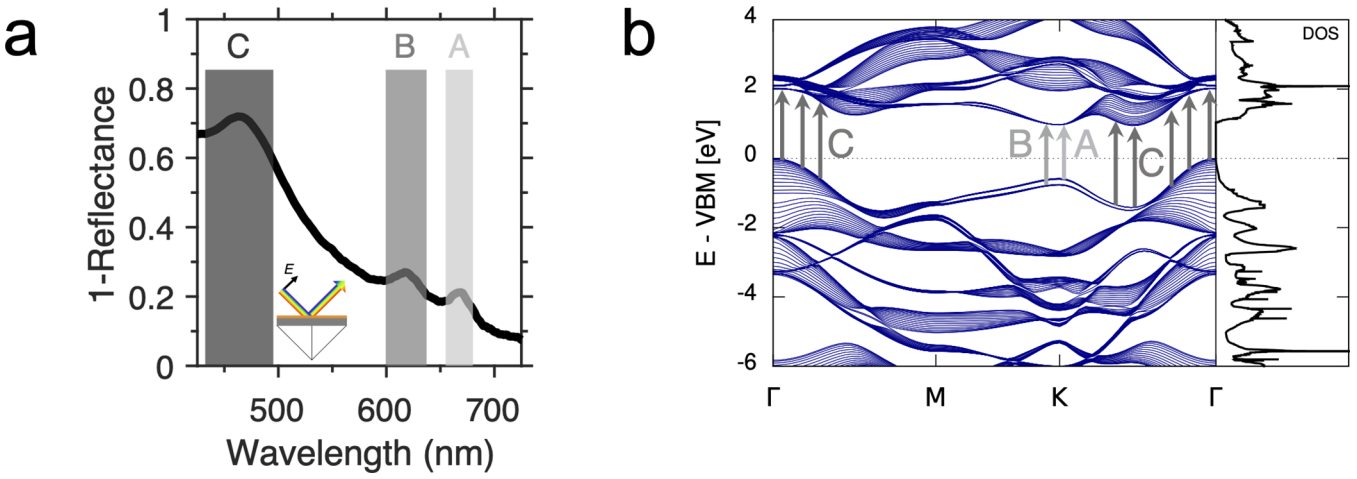

Figure 1. (a) Absorptivity (1 − reflectance) of ∼10 nm MoS_2 film on 40 nm Ag on glass. A, B, and C excitons are labeled by gray bands. Inset shows the reflection measurement schematic. (b) Band structure and density of states (DOS) of 16-layer MoS_2 (∼10 nm), calculated with density functional theory. A, B, and C excitons are labeled by gray arrows. A and B exciton transitions are between regions of the band structure with opposite concavity, whereas the C excitons are between parallel bands.

a unique feature of the TMDC band structure to maximize the coupling strength: the region of nested bands called the C exciton, highlighted in the absorption spectrum of Figure 1a. Whereas the lower-energy A and B excitons arise from bound transitions between the conduction band minimum and the spin−orbit-split valence band maxima at the K-point, the C exciton comes from regions of parallel or nested bands, as shown in Figure 1b, and therefore comprises a wealth of states. Band nesting is defined by equally spaced conduction and valence band energies over relatively wide regions of the band structure leading to numerous optically active transitions that result in a broad excitonic peak with large oscillator strength (Figure 1a). These collective states may be treated as a single Lorentzian oscillator and may therefore couple to polariton modes. Compared to bandgap excitons, carriers excited into nested bands are expected to have unique dynamics such as self-separation and intervalley scattering-limited lifetimes, possibly leading to slow carrier cooling as some have claimed to observe.[17,18] The possibility of slow cooling of hot (above bandgap) excitons makes 2D TMDCs candidates for hot carrier studies for photovoltaics or photoelectrochemistry where charge transfer may occur directly from high-lying states in the semiconductor to the contact or molecular reaction species. As a result, in hot carrier devices, the photovoltage is limited by the photon energy rather than the bandgap.

We hypothesize that under strong coupling, the C exciton lifetime will be prolonged. Such an effect has been observed in organic systems, where polariton modes live longer than bare states,[19,20] in part due to their photonic, delocalized nature, which enhances exciton and charge transport and decreases scattering (defect, phonon, intervalley, etc.).[8,11,21] To test this hypothesis, we use femtosecond pump−probe spectroscopy to observe the carrier dynamics of few-layer molybdenum disulfide (FL-MoS_2) under strong coupling of the C exciton with propagating surface plasmon polaritons (SPPs). We find the large oscillator strength of the C exciton pushes the coupling strength into the ultrastrong coupling regime, which will be discussed below. This ultrastrong coupling leads to significant increases in FL-MoS_2 lifetimes over the entire spectrum under study and especially for the lowest-energy exciton−polariton state relative to both the uncoupled C exciton and the ground state A exciton.

METHODS

Theoretical Calculations. In this work, we have calculated the band structure using *ab initio* density functional theory (DFT) methods to verify the band-nested structure in our 10 nm multilayer MoS_2 samples, as shown in Figure 1b. Although standard correlation functionals such as GGA−PBE used here tend to underestimate the bandgap, we expect the band profile to remain accurate. In comparing to previous G_0W_0 calculations on mono-to-few layer (1−6) MoS_2,[22] we find that the band profile remains similar. We looked at 16- and 17-layer (see Supporting Information (SI) Figure S1) structures to both span the 10 nm thickness of interest (calculated thicknesses of 9.7−10.3 nm) and account for any even- and odd-layer dependence in the band structure.[23]

All calculations were performed using DFT with the JDFTx[24] software implementation. The Perdew−Burke−Ernzerhof (PBE) form of the generalized gradient approximation was used to describe the exchange−correlation interaction. The valence electron−nuclear interactions were described by optimized fully relativistic norm-conserving Vanderbilt pseudopotentials (ONCVPSP)[25] from the Pseudo-Dojo Project[26] (stringent accuracy). A 45 Hartree cutoff was used for the plane-wave basis set. Calculations were performed with fully relativistic spin to capture the effects of spin−orbit coupling on the MoS_2 band structure. To capture the van der Waals interlayer interactions, the Grimme DFT + D2 scheme was used.[27]

The 16- and 17-layer MoS_2 slabs were constructed from lattice optimized bulk MoS_2. To prevent interaction between images, we employed a vacuum layer of at least 15 Å and truncated coulomb potentials[28] in the out-of-plane direction. The 2D multilayers were also allowed to fully relax to a final lattice parameter of 3.192 Å for both 16- and 17-layer structures and final thicknesses of 9.7 and 10.3 nm, respectively. To sample the Brillouin zone, a Γ-centered *k*-point sampling of 12 × 12 × 3 was used for the bulk, and 12 × 12 × 1 was used for the 2D multilayers. The convergence criteria were set to 1×10^{-6} Hartree for both the structure and

https://doi.org/10.1021/acs.jpcc.2c01262
J. Phys. Chem. C 2022, 126, 8710−8719

energy optimizations and converged via a variational minimization algorithm.[29] Finally, the density of states was obtained using the tetrahedron method for Brillouin zone integration.[30]

Fabrication. Samples were fabricated by depositing 1 nm of Ti and 40 nm of Ag without breaking vacuum via electron beam deposition onto a glass right angle prism (Edmund Optics 32−334, uncoated N-BK7 glass, 20 mm leg length).

FL-MoS_2 was grown by chemical vapor deposition on a sapphire substrate (University Wafer) and transferred to the Ag-coated prism. Spectroscopic ellipsometry (J. A. Woollam M-2000) was used to determine MoS_2 thickness of ∼10 nm. See Figure 2a for a representation of the sample. Details of the prism preparation, sample growth, and transfer are given in the SI.

Kretschmann−Raether Method. Thin film SPPs are optical excitations localized at the interface of metal−dielectric thin films and exhibit dispersion that is photonic ($\omega = ck$) at low energy and wavevector and asymptotically approaches a constant value at high energy and wavevector (see the extremes of Figure 2b). It is at the intersection of this plasmon dispersion and the dispersionless exciton modes that strong coupling may happen, as seen near 2.6−2.7 eV in Figure 2b.

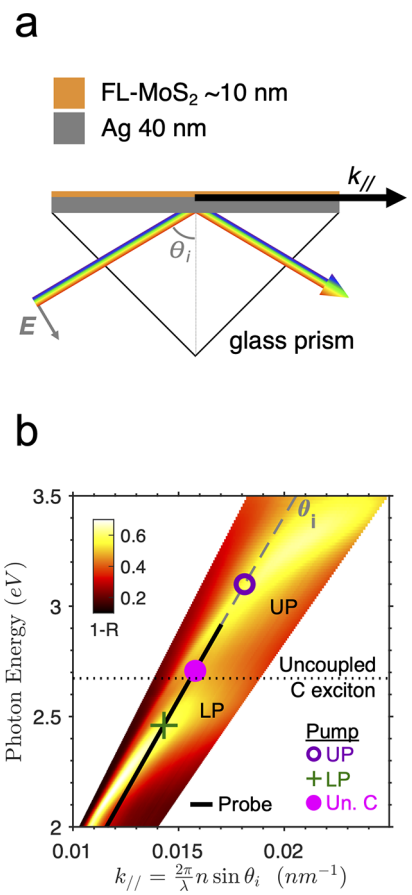

Figure 2. (a) Kretschmann−Raether (K−R) method of plasmon excitation for steady-state angle-resolved reflectance. Collimated plane-polarized white light excites the surface plasmon polariton through the backside of the glass prism, and reflected light is collected for a range of incident angles. (b) Steady-state dispersion of the strongly coupled Ag−MoS_2 system near the C exciton. K−R reflectance data, R, is converted to k-space dispersion by $k_{//} = (2\pi/\lambda)n\cdot\sin\theta_i$, where n is the refractive index of the glass prism. Color map shows the absorptivity = 1 − R. UP and LP stand for the upper and lower polariton branches, respectively. The dotted line shows the energy of the uncoupled C exciton, taken from its peak in Figure 1a. The dashed line shows the angle of incidence used for transient reflection (TR) experiments. The solid black line corresponds to the region of the dispersion plot probed in TR data sets. The TR pump energies at the incident angle are also labeled.

The optical dispersion was obtained by the Kretschmann−Raether (K−R) method, namely collecting plane-polarized angle-resolved reflectance through the backside of the prism, as shown in Figure 2a. For all excitation angles studied, light undergoes total internal reflection (TIR). A second glass prism with no coatings was used as a reflectance reference, as it exhibits near-unity reflectance under TIR while also accounting for interfacial reflection losses. Under TIR, transmission is negligible, and absorptivity, A, is related to reflectance, R, via $A = 1 - R$.

The dispersion is calculated as $k_{//} = (2\pi/\lambda)n\cdot\sin\theta_i$, where $k_{//}$ is the wavevector in the direction of SPP propagation and parallel to the surface of the prism, λ is the incident photon wavelength, n is the wavelength-dependent index of refraction of the prism, and θ_i is the incident angle of light inside the prism. The dispersion is calculated in MATLAB.[31] In this study, unless otherwise noted, the angle of incidence external to the prism was 51°, which corresponds to $\theta_i \cong 49°$ for wavelengths near the C exciton (additional data was taken at an external angle of incidence of 61°; see SI Figure S2 for the location of these data sets overlaid on the dispersion). All measurements were performed at room temperature in air.

Ultrafast Transient Reflection Spectroscopy. We performed femtosecond broadband transient reflection spectroscopy (TR) to characterize the dynamics of the system. The pump pulse was generated by passing the 1 kHz, 800 nm, (150 fs pulse width) output from a Coherent Libra Ti:sapphire laser into a TOPAS-C optical parametric amplifier where it was tuned to the desired wavelength (365 nm/3.4 eV; 400 nm/3.1 eV; 458 nm/2.71 eV; 504 nm/2.46 eV; and 652 nm/1.90 eV were used in this study). The probe pulse was generated by focusing a portion of the Ti:sapphire laser output onto a thin sapphire window to generate white light (440−775 nm). A portion of the probe pulse was picked off before the sample and used as a reference to reduce noise. The interval between the pump and probe pulses was controlled with a mechanical delay stage. The pump and probe beams are nearly colinear, spatially overlapped on the Ag−MoS_2 film, and excite the system in one of two configurations: (1) Excitation is from the top side of the prism (see Figure 3a) where plasmon excitation is disallowed due to the momentum mismatch between the photon in air and the surface plasmon, and behavior is independent of angle of excitation (at angles used for this study). This serves as a control for the behavior of MoS_2 on Ag and is referred to as the *control system*. (2) Excitation is through the backside of the prism (see Figure 3c), i.e., a pump−probe K−R configuration. This is referred to as the *coupled system*, except when we specifically pump the exciton reservoir, i.e., when we pump uncoupled states lying between the polariton modes, which we call the *uncoupled C exciton*. The TR data presented are differential reflectance (see SI for derivation). Pump fluence was maintained at $\lesssim$60 μJ/cm^2 and was controlled to maintain a similar maximum TR signal between data sets. The spectral region of the probe and pump energies at the angle of incidence studied are overlaid on the dispersion plot in Figure 2b. All measurements were performed at room temperature in air.

https://doi.org/10.1021/acs.jpcc.2c01262
J. Phys. Chem. C 2022, 126, 8710−8719

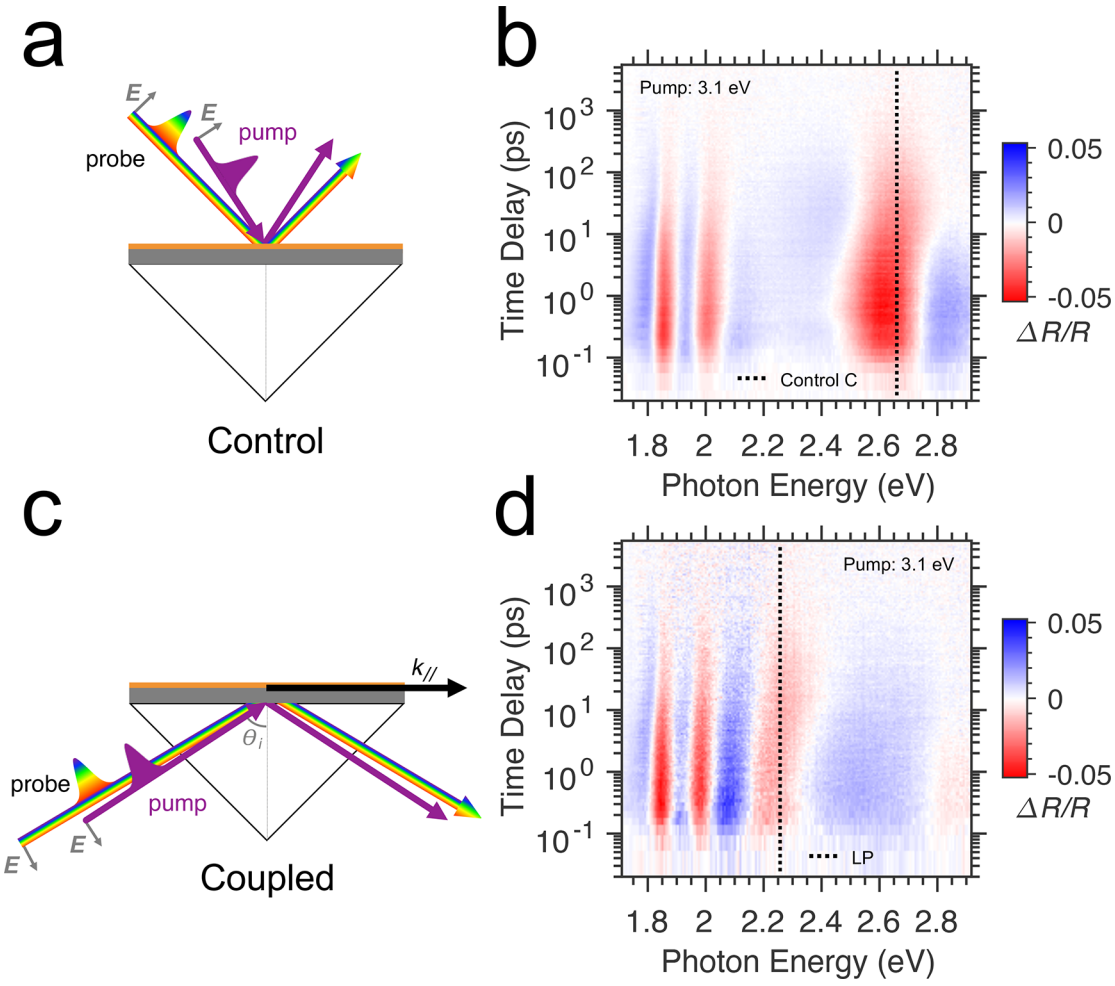

Figure 3. (a) Configuration of the pump−probe TR for the control case. Here, SPPs cannot be excited, and only uncoupled C excitons may be pumped or probed. (b) Plot of differential reflectance normalized to reflectance as a function of pump−probe time delay and incident probe photon energy for control case. Dotted line indicates the control C exciton feature probed in Figure 4a. (c) TR in the K−R configuration to the pump and probe coupled exciton−plasmon states. (d) Same as (b) but for the coupled case. Dotted line indicates the LP feature probed in Figure 4a,b (the UP pump is shown here; the LP feature and thus probe energy are shifted slightly for other pump energies).

Global Analysis. We use the transient spectroscopy analysis package Glotaran to globally fit the transient reflection data to a simple kinetic model.[5] First, singular value decomposition (SVD) is used to inspect the data and determine that three linear independent components fit the data well. The data is then modeled using a parallel decay scheme, where the three components are assumed to decay simultaneously, and the decay associated difference spectra (DADS) are obtained. The kinetic traces are given by a sum of three exponential decays convoluted with the instrument response function (IRF) where the amplitude of each exponential is given by the associated DADS.

RESULTS AND DISCUSSION

Ultrastrong Coupling at the C Exciton. Strong coupling can be observed in dispersion plots as two distinct coupled modes exhibiting anticrossing behavior at the intersection of the two uncoupled modes.[32] In Figure 2b, we observe two distinct coupled modes observed as two branches of increased absorptivity. The splitting of the bare plasmon occurs at the bare exciton energy E_C = 2.67 eV (taken from the C exciton peak of Figure 1a). The mode above this energy is termed the upper polariton (UP), while the mode below is termed the lower polariton (LP). The minimum energy separation between the mode peaks is called Rabi splitting, Ω, and is proportional to the coupling strength.

When the Rabi splitting is of the same order of magnitude as the bare exciton energy ($\Omega/E \gtrsim 10\%$), we enter the ultrastrong coupling regime,[32] which is notable for proposed emergent quantum physics such as ground state virtual photons and entangled pairs[33] but also important because conventional strong coupling effects are expected to be more efficient. (To be precise, ultrastrong coupling is defined in terms of coupling strength, whereas strong coupling is defined only for observable Rabi splitting; it is therefore technically possible to have ultrastrong coupling without visible Rabi splitting when the average oscillator widths are larger than the coupling strength. In this work, both definitions are met.)

The ultrastrong coupling regime is typically limited to organic systems,[20,34,35] and so far, nearly all work in the 2D TMDCs has shown relatively small Rabi splitting at the A and B excitons of ∼50−100 meV.[36−38] For example, our own work on very similar samples to those presented here but tuned for coupling to the A and B excitons showed Rabi splittings of 81 and 93 meV, which are 4.4 and 4.6% of their respective uncoupled exciton energies and therefore outside of the

https://doi.org/10.1021/acs.jpcc.2c01262
J. Phys. Chem. C 2022, 126, 8710−8719

ultrastrong coupling regime.[38] However, by exploiting the enhanced oscillator strength of the C exciton, we achieve Rabi splitting of Ω = 293 meV, which is 11.0% of the uncoupled exciton energy, placing it in the ultrastrong coupling regime. The Rabi splitting value is the result of fitting a semiclassical coupled harmonic oscillator model to the data and agrees within 1% of the experimentally determined minimum energy spacing between the peaks of the two branches (complete steady-state analysis details published elsewhere[39]).

Dynamics: Broadband Features. In Figure 3, we present the TR data for the control (Figure 3b) and coupled (Figure 3d) films. Analyzing thin film TR data is not straightforward, as it is sensitive to changes in both the real and imaginary components of the effective dielectric function.[19,40,41] Therefore, we cannot simply describe an increase in reflection (i.e., decrease in absorption) as a bleach due to state filling, for example. Even when studied using standard transient absorption, TMDC spectra are dominated by derivative-like features, which are mostly due to bandgap renormalization effects.[42] In our data, the kinetics generally follow those seen in MoS_2, such as a sub-ps decay attributed to thermalization and trapping of free carriers, followed by exponential decays on the order of 10 ps, 100 ps, and 1 ns attributed to various exciton recombination mechanisms from surface, grain boundary, or vacancy defects, exciton−exciton annihilation, radiative decay, and intervalley scattering.[18,43−48] After the initial sub-ps response, the spectral features seen in uncoupled MoS_2 are largely pump-independent and attributed almost completely to bandgap renormalization, which relaxes as excitons and free carriers relax.[42,49] While exciton−exciton annihilation is an important decay mechanism to consider in the bandgap region,[48,50,51] intervalley scattering is expected to be the limiting decay mechanism of the C exciton.[18]

In our analysis in the next two sections, we use two methods to analyze the data and compare kinetics. First, we ascribe the dominant negative TR features of Figure 3b,d to the excitons or polaritons and compare kinetics of these features among the coupled and uncoupled systems. Second, global analysis fitting of the kinetics corroborates the findings from the individual traces. We ascribe the negative features near 1.85 and 2.0 eV to the A and B excitons, respectively, noting that they look qualitatively similar between the two samples. Near the C exciton region, however, the difference in the samples is immediately obvious. In the control case, we see a strong negative feature near 2.6 eV that we assign to the C exciton. In the coupled sample, the C exciton feature splits into two negative features, which we assign to the two polariton modes. The UP negative feature is partially visible at energies greater than 2.8 eV, while the LP negative feature sits near 2.2 eV. Such a large split is indicative of being in the strong coupling regime.

We note that the plots shown in Figures 3b,d are excited at 3.1 eV (400 nm) and are qualitatively the same for the other pump energies used in this study (see SI Figure S3 for corresponding plots at additional pump energies); in the control case, they are nearly identical, and in the coupled case, there is some slight shifting of the polariton modes. Also, since the kinetics in MoS_2 is largely governed by bandgap renormalization, we expect to see a response from high-energy states even when the pump is comparatively low energy. Finally, we note that the dotted lines indicate the bare C exciton or LP features probed in the following sections, regardless of pump energy.

Dynamics: C Exciton. We start by comparing the kinetics of the control C exciton to the coupled sample when it is excited between the UP and LP (2.71 eV, pink filled circle in Figure 2b lying at the C exciton energy labeled by the dotted line)—that is, we excite the uncoupled C exciton state in both cases and thus expect to see similar kinetics. In Figure 4a, we

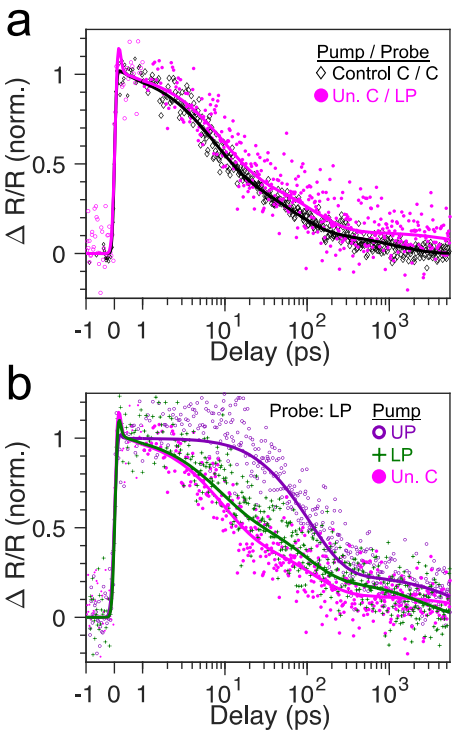

Figure 4. (a) Kinetics when pumping the uncoupled C exciton in control (black) and coupled samples (magenta). The pump in each case is at the peak of the C exciton, 2.71 eV (458 nm), which lies between the UP and LP in the coupled sample. (b) LP kinetics when pumping the UP (3.10 eV = 400 nm), LP (2.46 eV = 504 nm), or between the polaritons (2.71 eV = 458 nm). In (a) and (b), symbols are data, while lines are the global analysis fit; the features probed are those indicated with dotted lines in Figures 3b,d and 5. The pump energies are also indicated in Figure 2b. All data are normalized excluding the initial sub-ps feature.

show the kinetics, as probed at the C exciton or LP features. The data (symbols) is normalized excluding the sub-ps feature to focus on the long time scale behavior. Apart from the sub-ps feature, we do find similar kinetics between these two cases. Further, global analysis (solid lines) fits the data well in this region.

Furthermore, we highlight that in our control sample, when the C exciton is pumped, it lives significantly longer than the A exciton (whether or not the sub-ps response is excluded; see Figure S4). This is similar to a result seen by Wang et al. showing slow cooling of the C excitons and extraction of hot carriers in monolayer MoS_2.[17] However, the other literature on C exciton dynamics is collectively inconclusive about whether the C exciton lifetime is greater than the A or B excitons.[52−54,18] The differences between these studies could be due to differences in defect density and morphology of the samples. In the absence of many defects, though, the C exciton could be expected to have a longer lifetime than direct gap A and B excitons, because (1) the large momentum mismatch between the two regions leads to slow interband decay and (2)

https://doi.org/10.1021/acs.jpcc.2c01262
J. Phys. Chem. C 2022, 126, 8710−8719

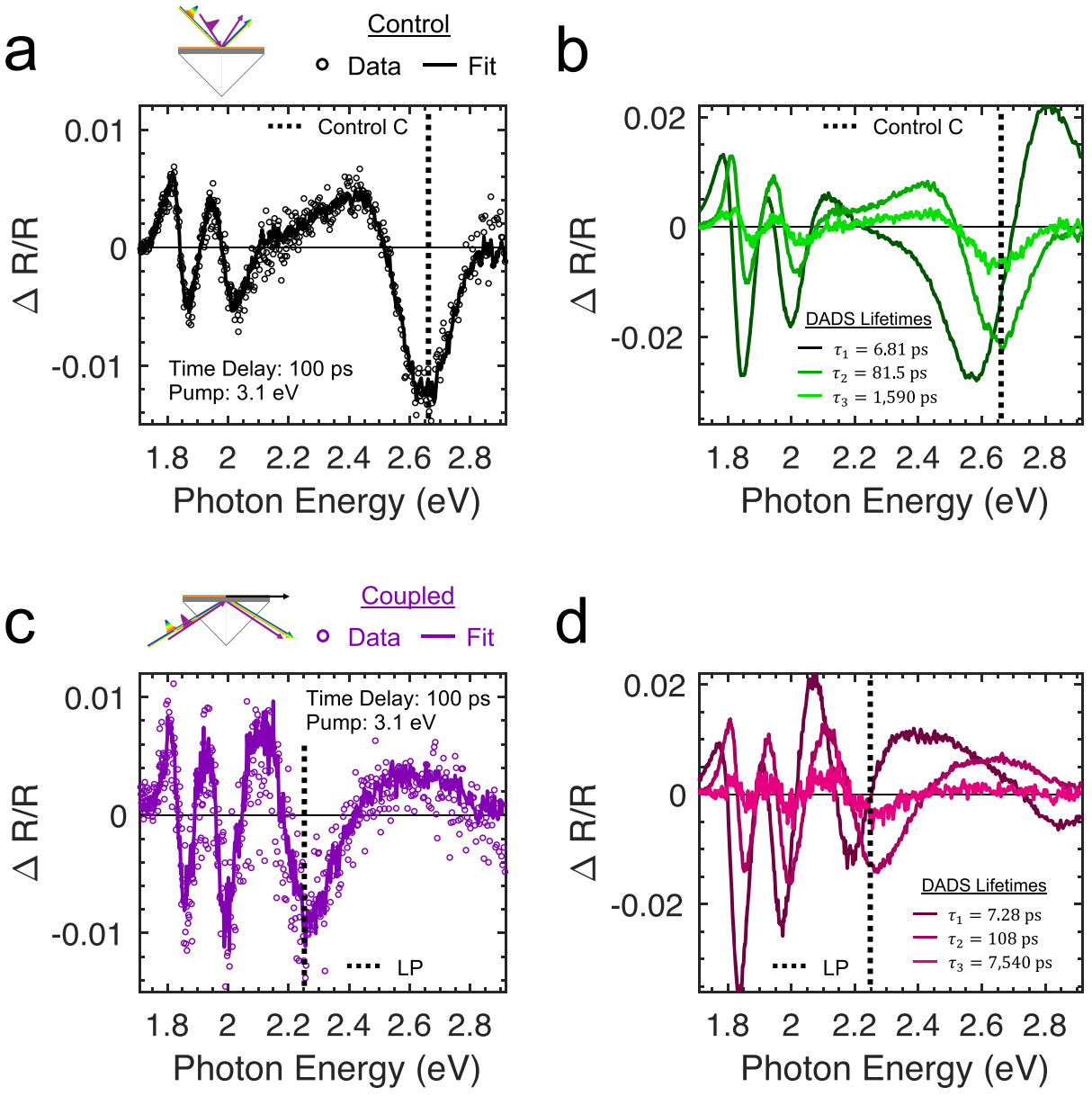

Figure 5. (a) TR spectrum for the control sample at 100 ps. (b) Control decay associated difference spectral (DADS) components found via global analysis. (c) TR spectrum for the coupled sample at 100 ps when UP is pumped. (d) DADS of the same coupled sample. In (a) and (c), open circles are data, while solid lines are the global analysis fit. Dotted lines indicate features probed in Figure 4 (note that the actual probe energy shifts slightly depending on pump).

the parallel bands induce charge separation in *k*-space, thereby reducing the probability of recombining via photon emission.

Dynamics: Polariton. Next, in Figure 4b, we consider how ultrastrong coupling affects the dynamics by pumping the polariton states. We compare the kinetics of the LP when we pump the coupled UP and LP states as well as the uncoupled C exciton again (i.e., the three pump energies shown in Figure 2b). When the LP is pumped, it shows slightly longer lifetimes than pumping the uncoupled states, up to ∼1 ns. The kinetics under the UP pump are strikingly different: the LP does not decay for the first ∼20 ps. While we do not know the origin of this quasiconstant region, we can hypothesize that this is the time constant associated with UP → LP decay, either directly or via intermediate states such as the uncoupled C exciton reservoir. Alternatively, the UP and LP states could decay independently of each other. This, however, seems unlikely, as the two are eigenstates of the same coherent exciton−polariton interaction. Unfortunately, fully probing the kinetics of the UP was not possible given the spectral range of our probe pulse and will have to be the subject of further experimentation.

To verify the conclusion that pumping the UP (3.1 eV) extends the lifetime of the LP compared to the bare C exciton, we compare the LP kinetics directly to the C exciton under the same pump condition. Figure S5 shows the kinetics, which also show that the polariton state lives dramatically longer than the bare state. We further compare the kinetics of the LP and A exciton in the coupled system under the UP pump, finding that the LP state lives significantly longer than the bandgap exciton (see Figure S6).

Altogether, these results indicate that ultrastrong coupling slows the cooling of hot excitons, likely through three mechanisms. First, the ∼20 ps UP → LP additional decay

https://doi.org/10.1021/acs.jpcc.2c01262
J. Phys. Chem. C 2022, 126, 8710−8719

Table 1. Exponential Decay Time Constants Extracted from Global Analysis[a]

	control						coupled					
pump	3.10 eV		2.71 eV		2.46 eV		3.10 eV (UP)		2.71 eV (un. C)		2.46 eV (LP)	
τ_1	6.81 ps	(1)	6.88 ps	(1)	8.21 ps	(1)	7.28 ps	(1)	8.94 ps	(1)	7.62 ps	(1)
τ_2	81.5 ps	(0.81)	63.9 ps	(0.56)	73.4 ps	(0.68)	108 ps	(1.27)	113 ps	(0.82)	88.5 ps	(0.69)
τ_3	1590 ps	(0.26)	1160 ps	(0.32)	1490 ps	(0.25)	7540 ps	(0.36)	12 200 ps	(0.27)	2680 ps	(0.38)

[a]Values in parentheses are the magnitude of the C exciton (control) or LP (coupled) feature for each DADS normalized to the τ_1 magnitude. Please see the SI for DADS spectra to view the relative contribution of each component throughout the spectrum. See the SI for the fitting routine error.

time under UP pumping can be understood as arising from the splitting of the C exciton into two hybrid states. Decaying hot carriers see this additional state as another hurdle, delaying their eventual decay. Second, as previously mentioned, reduced scattering is a known benefit of light−matter states, and thus, the LP lives longer under both UP and LP pumping. This polaritonic protection against scattering can be thought of as arising from delocalization: the excitons take on photonic character, and thus, their effective size approaches the order of the wavelength, which makes them insensitive to nanoscale defects.[8,11] Third, phonon-assisted intervalley scattering is also reduced. The hybrid modes are a coherent superposition of a photonic mode and an excitonic mode, but only the excitonic part interacts with phonon modes, and thus, intervalley scattering is reduced.[21] The weighting of each of these mechanisms is unknown.

Finally, we compare our results to ultrastrong coupling dynamics in organic systems. It has been noted that such systems do not obey Markovian dynamics, which are predicted by the simplest strong coupling theory. This theory predicts that the lifetime of coupled states, τ, should obey the relation $1/\tau = 1/\tau_{ph} + 1/\tau_{ex}$, where the photonic component τ_{ph}, having a short characteristic lifetime of femtoseconds, should dominate over the longer exciton lifetime τ_{ex}, and therefore, coupled exciton lifetimes should be much smaller than uncoupled.[55] However, like recent works on organic systems, we find that the lifetimes are increased over the bare excitons because of non-Markovian effects.[19,20,56,57] Theory suggests that one reason for the increased lifetimes is that the ground state of the strongly coupled system lies lower than that of the uncoupled system, thereby encouraging state filling of the coupled ground state.[57] Unlike organic systems though, we do not observe a fast decay of the UP to the LP and instead observe an appreciable increase in the lifetime of the UP. The fast UP → LP decay seen in organics is thought to be due to a high density of dark states between the polariton modes.[57] This implies that the FL-MoS_2 system studied here has fewer relaxation pathways between the polaritons.

Dynamics: Global Analysis. To corroborate the finding that ultrastrong coupling at the C exciton extends state lifetimes, we perform global analysis fitting of each data set. Figure 5a,c shows the data (open circles) and fits (solid lines) of the spectra at 100 ps for 3.1 eV (400 nm) excitation. The associated DADS are shown in Figure 5b,d with the fit lifetimes displayed on the plots. The approximate probe spectral positions of the kinetics shown in Figure 4 are marked by the dotted lines.

Examining Figure 5b at the C exciton feature, we find the fast time component is the largest component in the control sample; the magnitudes of the second and third component minima are 0.81 and 0.26 times as large as the first component, respectively. In the coupled sample, however (Figure 5d), among the LP features, the intermediate time constant is larger than the fast component; its magnitude is 1.27 times that of the first component, while the third component is a factor of 0.36 as large. Thus, in the coupled system, τ_2 and τ_3 account for a greater proportion of the decay dynamics. Further, we see in each case the coupled system lives longer: from shortest to longest, the ratio of coupled to control system time constants are 1.07, 1.33, and 4.74.

We find that while the lifetimes are pump-dependent, the coupled system time constants are almost universally longer than the control, as can be seen in Table 1. The one exception is τ_1 when pumping the LP. Interestingly, pumping the uncoupled C exciton reservoir of the coupled sample gives the longest lifetimes. However, proportionally more of the signal is in the short time component, leading to overall faster decay (see DADS in Figure S8) compared to pumping the polaritons. Nonetheless, theory has predicted uncoupled exciton states can take on polaritonic character in strongly coupled systems.[58] Indeed, the near universal extension of each time constant in the coupled system points to the polaritonic character causing a reduction in multiple types of scattering events, as described in the previous section.

To further support the conclusion the coupled system lifetimes are extended, we pump additional energies (365 nm/3.4 eV and 652 nm/1.90 eV) and a different region of the UP and LP (external angle of incidence of 61°, which corresponds to $\theta_i \cong 55°$; see SI Figures S2, S3, S7, and S8 and Table S1 for the location of all data sets overlaid on dispersion, TR data sets, global analysis fits at 100 ps, DADS, and extracted time constants, respectively, for all pump energies and angles studied). We find again that when pumping the polariton modes or the uncoupled exciton reservoir, the three lifetime components are extended in nearly each case. For all cases where the pump energy is ≥2.46 eV (504 nm), the average enhancement factors of the coupled system time constants, from shortest to longest, are 1.05, 1.50, and 5.82. Therefore, τ_2, which the literature assigns variously to surface, grain boundary, or vacancy defects, exciton−exciton annihilation, and intervalley scattering,[18,44,46−48] is extended by 50%, while τ_3, which is attributed to radiative decay from the A exciton,[48,52] is extended by a much greater amount (480%). One possible explanation for the discrepancy is that the nonradiative scattering events that lead to poor photoluminescence efficiency are more effectively screened by polariton coupling than τ_2 decay mechanisms. Recent work suggests that defect states enhance exciton−exciton annihilation (EEA),[59] so if EEA is the dominant decay mechanism at the A exciton, then polariton screening of defect states would also suppress EEA and therefore enhance radiative decay.

https://doi.org/10.1021/acs.jpcc.2c01262
J. Phys. Chem. C 2022, 126, 8710−8719

CONCLUSIONS

We studied the excited-state dynamics of FL-MoS_2 in conditions of light−matter hybridization. In the absence of strong coupling, we observed slow cooling of the C exciton compared to the bandgap A exciton, showing the promise of the 2D TMDCs for hot carrier devices. Under ultrastrong coupling to plasmon polaritons, this cooling was further slowed down by average factors of 1.05, 1.50, and 5.82 at three distinct time scales throughout the visible spectrum, when pumped near the hybrid states. This suggests that hybridizing the excitons with photonic modes suppresses multiple types of scattering events such as defects, intervalley scattering of band-nested excitations to the K-valleys, and exciton−exciton annihilation. We also saw evidence that opening a gap at the C exciton energy further prolonged decay of carriers excited into the new upper mode. Finally, our work extends recent observations of non-Markovian dynamics and long-lived coupled states in organic systems under ultrastrong coupling to the inorganic thin film TMDCs. Our results take a step toward achieving the efficient quantum coherent processes expected under ultrastrong coupling in the 2D TMDCs and has applications in hot carrier extraction for energy and chemical conversion.

ASSOCIATED CONTENT

Supporting Information

The Supporting Information is available free of charge at https://pubs.acs.org/doi/10.1021/acs.jpcc.2c01262.

Additional band structure calculation for 17-layer MoS_2, in-depth experimental and fabrication details, dispersion indicating the location of all data sets, additional TR data, kinetic traces, global analysis fits at 100 ps, DADS, and a table summarizing all fit decay constants (PDF)

AUTHOR INFORMATION

Corresponding Author

Jao van de Lagemaat − *National Renewable Energy Laboratory, Golden, Colorado 80401, United States;* orcid.org/0000-0001-5851-6163; Phone: (303) 384-6143; Email: Jao.vandeLagemaat@nrel.gov

Authors

Aaron H. Rose − *National Renewable Energy Laboratory, Golden, Colorado 80401, United States;* orcid.org/0000-0002-6603-8779

Taylor J. Aubry − *National Renewable Energy Laboratory, Golden, Colorado 80401, United States;* orcid.org/0000-0002-7639-8014

Hanyu Zhang − *National Renewable Energy Laboratory, Golden, Colorado 80401, United States;* Present Address: First Solar, 1035 Walsh Avenue, Santa Clara, California 95050, United States. (H.Z.); orcid.org/0000-0001-9942-8186

Derek Vigil-Fowler − *National Renewable Energy Laboratory, Golden, Colorado 80401, United States*

Complete contact information is available at: https://pubs.acs.org/10.1021/acs.jpcc.2c01262

Notes

The authors declare no competing financial interest.

ACKNOWLEDGMENTS

We would like to thank Melissa K. Gish of NREL for discussions. This work was authored by the National Renewable Energy Laboratory, operated by Alliance for Sustainable Energy, LLC, for the U.S. Department of Energy (DOE) under Contract No. DE-AC36-08GO28308. Funding provided by the U.S. Department of Energy Office of Science, Office of Basic Energy Sciences, Division of Chemical Sciences, Geosciences, and Biosciences, Solar Photochemistry Program. The views expressed in the article do not necessarily represent the views of the DOE or the U.S. Government.

REFERENCES

(1) Yokoyama, H. Physics and Device Applications of Optical Microcavities. *Science* **1992**, *256*, 66−70.

(2) Christopoulos, S.; von Högersthal, G. B. H.; Grundy, A. J. D.; Lagoudakis, P. G.; Kavokin, A. V.; Baumberg, J. J.; Christmann, G.; Butté, R.; Feltin, E.; Carlin, J.-F.; et al. Room-Temperature Polariton Lasing in Semiconductor Microcavities. *Phys. Rev. Lett.* **2007**, *98* (12), 126405.

(3) Zhao, J.; Su, R.; Fieramosca, A.; Zhao, W.; Du, W.; Liu, X.; Diederichs, C.; Sanvitto, D.; Liew, T. C. H.; Xiong, Q. Ultralow Threshold Polariton Condensate in a Monolayer Semiconductor Microcavity at Room Temperature. *Nano Lett.* **2021**, *21* (7), 3331−3339.

(4) Thomas, A.; George, J.; Shalabney, A.; Dryzhakov, M.; Varma, S. J.; Moran, J.; Chervy, T.; Zhong, X.; Devaux, E.; Genet, C.; et al. Ground-State Chemical Reactivity under Vibrational Coupling to the Vacuum Electromagnetic Field. *Angew. Chem.* **2016**, *128* (38), 11634−11638.

(5) Thomas, A.; Lethuillier-Karl, L.; Nagarajan, K.; Vergauwe, R. M. A.; George, J.; Chervy, T.; Shalabney, A.; Devaux, E.; Genet, C.; Moran, J.; et al. Tilting a Ground-State Reactivity Landscape by Vibrational Strong Coupling. *Science* **2019**, *363* (6427), 615−619.

(6) Mandal, A.; Krauss, T. D.; Huo, P. Polariton-Mediated Electron Transfer via Cavity Quantum Electrodynamics. *J. Phys. Chem. B* **2020**, *124* (29), 6321−6340.

(7) Deng, M.; Wang, X.; Chen, J.; Li, Z.; Xue, M.; Zhou, Z.; Lin, F.; Zhu, X.; Fang, Z. Plasmonic Modulation of Valleytronic Emission in Two-Dimensional Transition Metal Dichalcogenides. *Adv. Funct. Mater.* **2021**, *31* (20), 2010234.

(8) DelPo, C. A.; Khan, S.-U.-Z.; Park, K. H.; Kudisch, B.; Rand, B. P.; Scholes, G. D. Polariton Decay in Donor-Acceptor Cavity Systems. *J. Phys. Chem. Lett.* **2021**, *12*, 9774−9782.

(9) Byrnes, T.; Kim, N. Y.; Yamamoto, Y. Exciton-Polariton Condensates. *Nat. Phys.* **2014**, *10* (11), 803−813.

(10) Hutchison, J. A.; Liscio, A.; Schwartz, T.; Canaguier-Durand, A.; Genet, C.; Palermo, V.; Samorì, P.; Ebbesen, T. W. Tuning the Work-Function Via Strong Coupling. *Adv. Mater.* **2013**, *25* (17), 2481−2485.

(11) Orgiu, E.; George, J.; Hutchison, J. A.; Devaux, E.; Dayen, J. F.; Doudin, B.; Stellacci, F.; Genet, C.; Schachenmayer, J.; Genes, C.; et al. Conductivity in Organic Semiconductors Hybridized with the Vacuum Field. *Nat. Mater.* **2015**, *14* (11), 1123−1129.

(12) Pockrand, I.; Swalen, J. D. Anomalous Dispersion of Surface Plasma Oscillations. *J. Opt. Soc. Am.* **1978**, *68* (8), 1147−1151.

(13) Gómez, D. E.; Vernon, K. C.; Mulvaney, P.; Davis, T. J. Coherent Superposition of Exciton States in Quantum Dots Induced by Surface Plasmons. *Appl. Phys. Lett.* **2010**, *96* (7), 073108.

(14) Skolnick, M. S.; Fisher, T. A.; Whittaker, D. M. Strong Coupling Phenomena in Quantum Microcavity Structures. *Semicond. Sci. Technol.* **1998**, *13* (7), 645−669.

(15) Vitale, S. A.; Nezich, D.; Varghese, J. O.; Kim, P.; Gedik, N.; Jarillo-Herrero, P.; Xiao, D.; Rothschild, M. Valleytronics: Opportunities, Challenges, and Paths Forward. *Small* **2018**, *14* (38), 1801483.

(16) Goh, K. E. J.; Bussolotti, F.; Lau, C. S.; Kotekar-Patil, D.; Ooi, Z. E.; Chee, J. Y. Toward Valley-Coupled Spin Qubits. *Adv. Quantum Technol.* **2020**, *3* (6), 1900123.
(17) Wang, L.; Wang, Z.; Wang, H.-Y.; Grinblat, G.; Huang, Y.-L.; Wang, D.; Ye, X.-H.; Li, X.-B.; Bao, Q.; Wee, A.-S.; et al. Slow Cooling and Efficient Extraction of C-Exciton Hot Carriers in MoS_2 Monolayer. *Nat. Commun.* **2017**, *8*, 13906.
(18) Li, Y.; Shi, J.; Chen, H.; Mi, Y.; Du, W.; Sui, X.; Jiang, C.; Liu, W.; Xu, H.; Liu, X. Slow Cooling of High-Energy C Excitons Is Limited by Intervalley-Transfer in Monolayer MoS_2. *Laser Photonics Rev.* **2019**, *13* (4), 1800270.
(19) Schwartz, T.; Hutchison, J. A.; Léonard, J.; Genet, C.; Haacke, S.; Ebbesen, T. W. Polariton Dynamics under Strong Light-Molecule Coupling. *ChemPhysChem* **2013**, *14* (1), 125−131.
(20) Wang, S.; Chervy, T.; George, J.; Hutchison, J. A.; Genet, C.; Ebbesen, T. W. Quantum Yield of Polariton Emission from Hybrid Light-Matter States. *J. Phys. Chem. Lett.* **2014**, *5* (8), 1433−1439.
(21) Chen, Y.-J.; Cain, J. D.; Stanev, T. K.; Dravid, V. P.; Stern, N. P. Valley-Polarized Exciton-Polaritons in a Monolayer Semiconductor. *Nat. Photonics* **2017**, *11* (7), 431−435.
(22) Hu, J.-Q.; Shi, X.-H.; Wu, S.-Q.; Ho, K.-M.; Zhu, Z.-Z. Dependence of Electronic and Optical Properties of MoS_2 Multilayers on the Interlayer Coupling and Van Hove Singularity. *Nanoscale Res. Lett.* **2019**, *14* (1), 288.
(23) Wu, Z.; Xu, S.; Lu, H.; Khamoshi, A.; Liu, G.-B.; Han, T.; Wu, Y.; Lin, J.; Long, G.; He, Y.; et al. Even-Odd Layer-Dependent Magnetotransport of High-Mobility Q-Valley Electrons in Transition Metal Disulfides. *Nat. Commun.* **2016**, *7* (1), 12955.
(24) Sundararaman, R.; Letchworth-Weaver, K.; Schwarz, K. A.; Gunceler, D.; Ozhabes, Y.; Arias, T. A. JDFTx: Software for Joint Density-Functional Theory. *SoftwareX* **2017**, *6*, 278−284.
(25) Hamann, D. R. Optimized Norm-Conserving Vanderbilt Pseudopotentials. *Phys. Rev. B* **2013**, *88* (8), 085117.
(26) van Setten, M. J.; Giantomassi, M.; Bousquet, E.; Verstraete, M. J.; Hamann, D. R.; Gonze, X.; Rignanese, G.-M. The PseudoDojo: Training and Grading a 85 Element Optimized Norm-Conserving Pseudopotential Table. *Comput. Phys. Commun.* **2018**, *226*, 39−54.
(27) Grimme, S. Semiempirical GGA-Type Density Functional Constructed with a Long-Range Dispersion Correction. *J. Comput. Chem.* **2006**, *27* (15), 1787−1799.
(28) Sundararaman, R.; Arias, T. A. Regularization of the Coulomb Singularity in Exact Exchange by Wigner-Seitz Truncated Interactions: Towards Chemical Accuracy in Nontrivial Systems. *Phys. Rev. B* **2013**, *87* (16), 165122.
(29) Arias, T. A.; Payne, M. C.; Joannopoulos, J. D. *Ab Initio* Molecular Dynamics: Analytically Continued Energy Functionals and Insights into Iterative Solutions. *Phys. Rev. Lett.* **1992**, *69* (7), 1077−1080.
(30) Lehmann, G.; Taut, M. On the Numerical Calculation of the Density of States and Related Properties. *Phys. Status Solidi B* **1972**, *54* (2), 469−477.
(31) Rose, A. H. *RTACalc 2 (MATLAB code)*. https://github.com/rose3fa/RTACalc (accessed 2022-02-13).
(32) Törmä, P.; Barnes, W. L. Strong Coupling between Surface Plasmon Polaritons and Emitters: A Review. *Rep. Prog. Phys.* **2015**, *78*, 013901.
(33) Frisk Kockum, A.; Miranowicz, A.; De Liberato, S.; Savasta, S.; Nori, F. Ultrastrong Coupling between Light and Matter. *Nat. Rev. Phys.* **2019**, *1* (1), 19−40.
(34) Thomas, P. A.; Menghrajani, K. S.; Barnes, W. L. Cavity-Free Ultrastrong Light-Matter Coupling. *J. Phys. Chem. Lett.* **2021**, *12* (29), 6914−6918.
(35) Bujalance, C.; Esteso, V.; Caliò, L.; Lavarda, G.; Torres, T.; Feist, J.; García-Vidal, F. J.; Bottari, G.; Míguez, H. Ultrastrong Exciton-Photon Coupling in Broadband Solar Absorbers. *J. Phys. Chem. Lett.* **2021**, *12* (43), 10706−10712.
(36) Liu, W.; Lee, B.; Naylor, C. H.; Ee, H.-S.; Park, J.; Johnson, A. T. C.; Agarwal, R. Strong Exciton-Plasmon Coupling in MoS_2 Coupled with Plasmonic Lattice. *Nano Lett.* **2016**, *16* (2), 1262−1269.
(37) Cuadra, J.; Baranov, D. G.; Wersäll, M.; Verre, R.; Antosiewicz, T. J.; Shegai, T. Observation of Tunable Charged Exciton Polaritons in Hybrid Monolayer WS_2-Plasmonic Nanoantenna System. *Nano Lett.* **2018**, *18* (3), 1777−1785.
(38) Rose, A. H.; Dunklin, J. R.; Zhang, H.; Merlo, J. M.; van de Lagemaat, J. Plasmon-Mediated Coherent Superposition of Discrete Excitons under Strong Exciton-Plasmon Coupling in Few-Layer MoS_2 at Room Temperature. *ACS Photonics* **2020**, *7* (5), 1129−1134.
(39) Rose, A. H.; Aubry, T. J.; Zhang, H.; van de Lagemaat, J. Ultrastrong Coupling of Band-Nested Excitons in Few-Layer Molybdenum Disulphide. *arXiv*, 2022. arXiv:2204.13768 [cond-mat.mes-hall].
(40) Yang, Y.; Yang, M.; Moore, D. T.; Yan, Y.; Miller, E. M.; Zhu, K.; Beard, M. C. Top and Bottom Surfaces Limit Carrier Lifetime in Lead Iodide Perovskite Films. *Nat. Energy* **2017**, *2* (2), 16207.
(41) Ashoka, A.; Tamming, R. R.; Girija, A. V.; Bretscher, H.; Verma, S. D.; Yang, S.-D.; Lu, C.-H.; Hodgkiss, J. M.; Ritchie, D.; Chen, C. et al. Extracting Quantitative Dielectric Properties from Pump-Probe Spectroscopy. *arXiv*, 2021. arXiv:2108.10605 [physics.app-ph].
(42) Pogna, E. A. A.; Marsili, M.; De Fazio, D.; Dal Conte, S.; Manzoni, C.; Sangalli, D.; Yoon, D.; Lombardo, A.; Ferrari, A. C.; et al. Photo-Induced Bandgap Renormalization Governs the Ultrafast Response of Single-Layer MoS_2. *ACS Nano* **2016**, *10* (1), 1182−1188.
(43) Nie, Z.; Long, R.; Sun, L.; Huang, C.-C.; Zhang, J.; Xiong, Q.; Hewak, D. W.; Shen, Z.; Prezhdo, O. V.; Loh, Z.-H. Ultrafast Carrier Thermalization and Cooling Dynamics in Few-Layer MoS_2. *ACS Nano* **2014**, *8* (10), 10931−10940.
(44) Wang, H.; Zhang, C.; Rana, F. Surface Recombination Limited Lifetimes of Photoexcited Carriers in Few-Layer Transition Metal Dichalcogenide MoS_2. *Nano Lett.* **2015**, *15* (12), 8204−8210.
(45) Cunningham, P. D.; McCreary, K. M.; Hanbicki, A. T.; Currie, M.; Jonker, B. T.; Hayden, L. M. Charge Trapping and Exciton Dynamics in Large-Area CVD Grown MoS_2. *J. Phys. Chem. C* **2016**, *120* (10), 5819−5826.
(46) Dunklin, J. R.; Zhang, H.; Yang, Y.; Liu, J.; van de Lagemaat, J. Dynamics of Photocatalytic Hydrogen Production in Aqueous Dispersions of Monolayer-Rich Tungsten Disulfide. *ACS Energy Lett.* **2018**, *3* (9), 2223−2229.
(47) Schiettecatte, P.; Geiregat, P.; Hens, Z. Ultrafast Carrier Dynamics in Few-Layer Colloidal Molybdenum Disulfide Probed by Broadband Transient Absorption Spectroscopy. *J. Phys. Chem. C* **2019**, *123* (16), 10571−10577.
(48) Sun, D.; Rao, Y.; Reider, G. A.; Chen, G.; You, Y.; Brézin, L.; Harutyunyan, A. R.; Heinz, T. F. Observation of Rapid Exciton-Exciton Annihilation in Monolayer Molybdenum Disulfide. *Nano Lett.* **2014**, *14* (10), 5625−5629.
(49) Carroll, G. M.; Zhang, H.; Dunklin, J. R.; Miller, E. M.; Neale, N. R.; van de Lagemaat, J. Unique Interfacial Thermodynamics of Few-Layer 2D MoS_2 for (Photo)Electrochemical Catalysis. *Energy Environ. Sci.* **2019**, *12* (5), 1648−1656.
(50) Mouri, S.; Miyauchi, Y.; Toh, M.; Zhao, W.; Eda, G.; Matsuda, K. Nonlinear Photoluminescence in Atomically Thin Layered WSe_2 Arising from Diffusion-Assisted Exciton-Exciton Annihilation. *Phys. Rev. B* **2014**, *90* (15), 155449.
(51) Yuan, L.; Huang, L. Exciton Dynamics and Annihilation in WS_2 2D Semiconductors. *Nanoscale* **2015**, *7* (16), 7402−7408.
(52) Shi, H.; Yan, R.; Bertolazzi, S.; Brivio, J.; Gao, B.; Kis, A.; Jena, D.; Xing, H. G.; Huang, L. Exciton Dynamics in Suspended Monolayer and Few-Layer MoS_2 2D Crystals. *ACS Nano* **2013**, *7* (2), 1072−1080.
(53) Kozawa, D.; Kumar, R.; Carvalho, A.; Kumar Amara, K.; Zhao, W.; Wang, S.; Toh, M.; Ribeiro, R. M.; Castro Neto, A. H.; Matsuda, K.; et al. Photocarrier Relaxation Pathway in Two-Dimensional Semiconducting Transition Metal Dichalcogenides. *Nat. Commun.* **2014**, *5* (1), 4543.

https://doi.org/10.1021/acs.jpcc.2c01262
J. Phys. Chem. C 2022, 126, 8710−8719

(54) Borzda, T.; Gadermaier, C.; Vujicic, N.; Topolovsek, P.; Borovsak, M.; Mertelj, T.; Viola, D.; Manzoni, C.; Pogna, E. A. A.; Brida, D.; et al. Charge Photogeneration in Few-Layer MoS_2. *Adv. Funct. Mater.* **2015**, *25* (22), 3351−3358.
(55) Ebbesen, T. W. Hybrid Light-Matter States in a Molecular and Material Science Perspective. *Acc. Chem. Res.* **2016**, *49* (11), 2403−2412.
(56) Virgili, T.; Coles, D.; Adawi, A. M.; Clark, C.; Michetti, P.; Rajendran, S. K.; Brida, D.; Polli, D.; Cerullo, G.; Lidzey, D. G. Ultrafast Polariton Relaxation Dynamics in an Organic Semiconductor Microcavity. *Phys. Rev. B* **2011**, *83* (24), 245309.
(57) Canaguier-Durand, A.; Genet, C.; Lambrecht, A.; Ebbesen, T. W.; Reynaud, S. Non-Markovian Polariton Dynamics in Organic Strong Coupling. *Eur. Phys. J. D* **2015**, *69* (1), 24.
(58) Gonzalez-Ballestero, C.; Feist, J.; Gonzalo Badía, E.; Moreno, E.; Garcia-Vidal, F. J. Uncoupled Dark States Can Inherit Polaritonic Properties. *Phys. Rev. Lett.* **2016**, *117* (15), 156402.
(59) Zhang, T.; Wang, J. Defect-Enhanced Exciton-Exciton Annihilation in Monolayer Transition Metal Dichalcogenides at High Exciton Densities. *ACS Photonics* **2021**, *8* (9), 2770−2780.

https://doi.org/10.1021/acs.jpcc.2c01262
J. Phys. Chem. C 2022, 126, 8710−8719